Available online at www.sciencedirect.com
ScienceDirect
Journal of Power Sources 176 (2008) 293–298
JOURNAL OF POWER SOURCES
www.elsevier.com/locate/jpowsour

Short communication

Performance of a metallic gas diffusion layer for PEM fuel cells

Feng-Yuan Zhang *, Suresh G. Advani, Ajay K. Prasad

Fuel Cell Research Laboratory, Department of Mechanical Engineering, University of Delaware, Newark, DE 19716-3140, USA

Received 8 September 2007; received in revised form 12 October 2007; accepted 12 October 2007
Available online 26 October 2007

Abstract

A novel metallic porous medium with improved thermal and electrical conductivities and controllable porosity was developed based on micro/nano technology for its potential application in PEM fuel cells. In this work to demonstrate its applicability, the gas diffusion medium, made of 12.5 μm thick copper foil, was tested in an operational fuel cell. The small thickness and straight-pore feature of this novel material provides improved water management even at low flow rates. The performance does not decline at lower flow rates, unlike conventional gas diffusion layers. It has been shown that the performance can be further enhanced by increasing the in-plane transport. The improvements of such gas diffusion layer, including pore shape, porosity, and surface properties, are fully discussed.

Keywords: PEM fuel cell; Gas diffusion layer; Micro/nano fabrication; Wet etching; Self-assembled monolayers

1. Introduction

The fuel cell offers the potential to become an attractive power system due to its high efficiency, low pollution, and low noise, however its cost is a major barrier for commercialization to date [1]. A fuel cell mainly consists of bipolar plates, gas diffusion layers (GDL), and a membrane electrode assembly (MEA). The performance and durability of fuel cells are significantly impacted by the GDL characteristics, whose principal functions are to efficiently transport reactants and products to and from the reaction sites, as well as to conduct heat and electric current. Current GDL materials, which include carbon cloth or paper, have shown limited success [2] as they do not meet long-term requirements for fuel cell performance, durability, and cost. During operation, water is produced on the cathode catalyst layer and is transported mainly through the GDL, and is finally removed through the flow channel [3–10]. The excess product water (in excess of the amount required to keep the reactants and PEM saturated) must be removed in order to prevent blockage of the flow field channels and flooding of the GDL and catalyst layer that could prevent reactant gases from reaching the reaction sites [11–18].

Conventional GDLs have arbitrary micro-structure and small pore size, especially under compression, which can require larger capillary pressures to drive liquid water through. Consequently, the GDL and catalyst layer in practical PEM fuel cells undergo flooding [3,8–13,18]. The key issues of flooding and mass transport limitation under steady-state and transient (e.g., start-up) conditions will benefit significantly from GDLs with carefully designed architectures and controlled pore-size distribution. It has also been shown that if the pores were straight and not interconnected, the liquid water would freely drain out of the GDL once the water flow was initiated [8,19,20]. Such a careful optimization of pore morphology and pore-size distribution is difficult to achieve in conventional GDLs due to the random distribution of carbon fibers. Furthermore, conventional GDLs are typically made hydrophobic by treating them with PTFE, which increases their weight by 5 to 30% and also reduces their electronic and thermal conductivities. In addition, GDLs made from carbon cloth or carbon paper are subjected to compressive stresses which reduces their thickness, and decreases their porosity and permeability by up to 50%. These conditions also

* Corresponding author. Tel.: +1 302 831 8796; fax: +1 302 831 3619.
E-mail address: fyzhang@udel.edu (F.-Y. Zhang).

0378-7753/$ – see front matter © 2007 Elsevier B.V. All rights reserved.
doi:10.1016/j.jpowsour.2007.10.055

limit the durability of the GDL and consequently the fuel cell [21–23].

With the rapid development of MEMS/nanotechnology, several avenues for improving GDL thermal and electrical conductivity, mass transport, and permeability are being explored. MEMS/nanotechnology provides advantages such as high precision, good repeatability, and automated batch-production. In addition, micro/nano fabrication equipment can easily etch patterns with high feature resolution on metals with high thermal and electric conductivities, which are key functional requirements of the GDL in PEMFCs. More importantly, wet etching provides a low-cost method, and it can result in a faithful transfer of the pattern on the underlying metal with the help of a patterned mask [24–27]. In this work, a copper foil was fabricated into a porous medium as a replacement for a conventional GDL, and its performance was evaluated in an operational fuel cell. Also, techniques for improving fuel cell performance with such novel materials are developed and discussed.

2. Experimental details

The novel gas diffusion medium was fabricated using 12.5 μm-thick copper foil (Cu110). The process mainly consists of mask design, pattern development, and etching at room temperature. The initial step consists of bonding the copper foil on to a standard silicon (Si) wafer by applying a sacrificial layer of photoresist material (SPR220) to the Si surface. Next, another layer of photoresist S1813 is applied on the Cu surface followed by a soft-baking process on a 90 °C hot plate for 2 min. The S1813 photoresist is patterned with a mask aligner, and subsequently developed in AZ 300 MIF developer for 2 min. To improve mask stability, adhesion, and chemical resistance, a hard bake was performed for 10 min at 120 °C. The wafer with copper foils then dipped into the copper etchant at room temperature. Finally, the copper foil GDL is released using a lift-off process, and then thoroughly rinsed with deionized water and dried. Detailed information on the fabrication process can be found in Ref. [28]. The patterned mask and etched pattern were examined with an Olympus BX60/U-CFU real time confocal microscope. A JSM-7400F field emission scanning electron microscope (FESEM) was used to examine the cross section of the etched trench and small features with high spatial resolution.

Two self-assembled monolayers (SAMs) with octadecanethiol (ODT, HS(CH2)17CH3) and 11-hydroxy-1-undecanethiol (HS(CH2)11OH) (all from Aldrich) were applied to the copper foil GDL to control their surface properties. The SAMs were prepared by incubating the cleaned copper samples in an ethanol solution of 2 mM ODT and 11-hydroxy-1-undecanethiol for about 8 h and 15 h, respectively. After treatment, the sample was removed from the solution and rinsed with ethanol. The solvent surfaces were then dried off with nitrogen.

The experimental setup for the PEMFC consists of a 10 cm^2 standard fuel cell (Fuel Cell Technology) and a 200-W test stand (Arbin Instruments) with controlled temperature, pressure, gas flow rate and relative humidity, an electronic load and a data acquisition system. The catalyst-coated membrane was Nafion-based, 25 μm thick, with Pt catalyst loading of 0.3 mg cm^{-2} on each electrode. As shown in Fig. 1, it was sandwiched between two gas diffusion layers, SGL 31 BA on the anode side, and the fabricated copper GDL on the cathode side. The fuel cell was operated at 70 °C, with fully humidified inlet air and hydrogen. The operating pressure was 2 atm (abs). In all the experiments, ultra-high purity (>99.999%) hydrogen and standard dry air were used from compressed gas bottles.

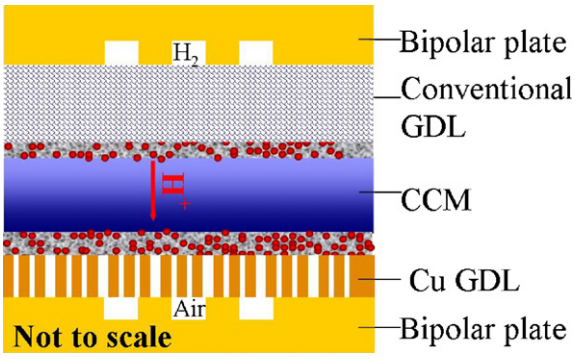

Fig. 1. Schematic of fuel cells with Cu gas diffusion layer.

3. Results and discussion

Fig. 2 shows an SEM image of the copper GDL after 20 min of etching. The number inside the pore indicates the mask width in μm. The pore distribution of mask widths with 20 μm, 15 μm, 10 μm, 8 μm and 5 μm relative to the number density at 20 μm is 1, 1, 8, 54, and 64, respectively. The mean pore size after etching for 20 min is 35.65 μm, while the porosity of the copper GDL is about 21%. It should be noted here that the mean pore size and porosity could be changed by altering the mask width, varying the etching time, and changing the pore distributions, which will be discussed later.

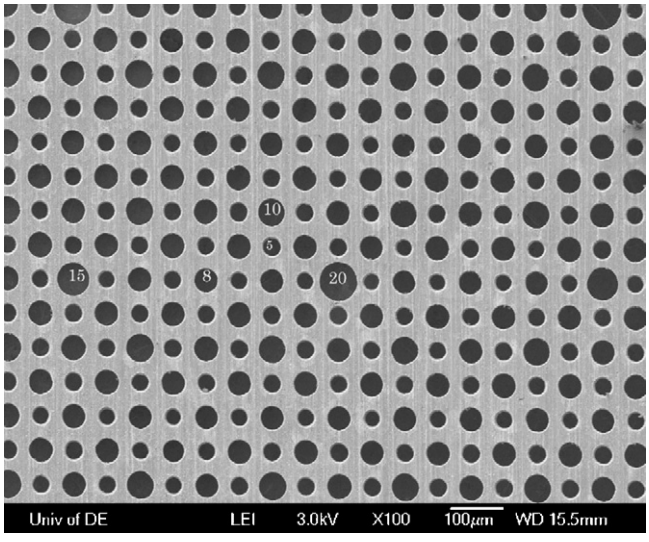

Fig. 2. Typical SEM image of the copper GDM after 20 min of etching. Reproduced from Ref. [28] with permission from the Institute of Physics.

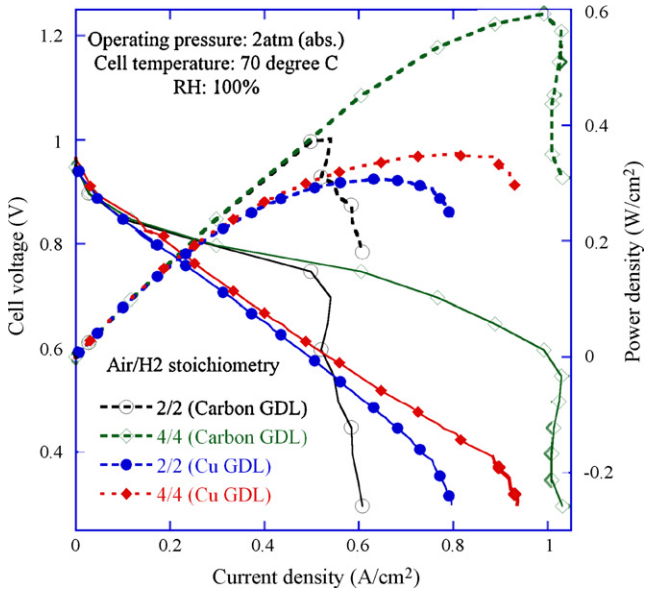

Fig. 3. Polarization curves of the fuel cell using copper gas diffusion medium and carbon paper under stoichiometry of 4/4 and 2/2 at 1 A cm^{-2}.

Fig. 3 shows the polarization curves of the fuel cell using both the copper GDL (closed symbols), and Toray TGP-H-060 carbon paper for comparison (open symbols), under stoichiometries of 4/4 and 2/2 at 1 A cm^{-2}. The dashed lines represent the power density, and the solid lines represent the cell voltage. The curves more or less overlap at lower current densities, whereas the performance improves with flow stoichiometry at higher current densities due to improved mass transport [3–5,8–11,30]. As shown in the figure, power density for the copper GDL peaks at 0.35 W cm^{-2} at a stoichiometry of 4/4, while even at the lower stoichiometry of 2/2, the maximum power density recorded was 0.3 W cm^{-2}. On the other hand for conventional GDL with Toray TGP-H-060, the peaks of power density are 0.59 W cm^{-2} and 0.39 W cm^{-2}, respectively. Although the copper GDL has lower performance (for reasons to be addressed subsequently), it can be seen that the performance of the metallic GDL does not decline as much at the lower flow rate, unlike conventional GDLs which can experience up to 30% reduction. The small thickness and straight-pore feature of this novel material provides improved water management even at low flow rate. The liquid water can be easily removed from the GDL and the flooding time in the GDL is also greatly reduced due to the small thickness.

Next, a microporous layer (MPL) was applied on the copper GDL to improve fuel cell performance. To form the MPL, 1 g of carbon powder (Vulcan XC-72), 0.2 g of Triton X-100, 1.1 g of PTFE (60 wt.%), 10 g of DI water and 10 g of isopropyl alcohol (IPA) as a pore-former were mechanically mixed. The resulting carbon ink was spray-deposited onto one side of the cleaned copper GDL. Then it was dried at 80 °C for 30 min and was sintered in a vacuum oven at 360 °C for 1 h [31–33].

Fig. 4 shows a typical SEM image of the in-house fabricated MPL on the metallic GDL. As shown in the upper-right corner of Fig. 4, the MPL surface is very hydrophobic with a contact angle of about 152°. In addition, compared with the mean pore size of the copper GDL of 35.65 μm, the MPL's

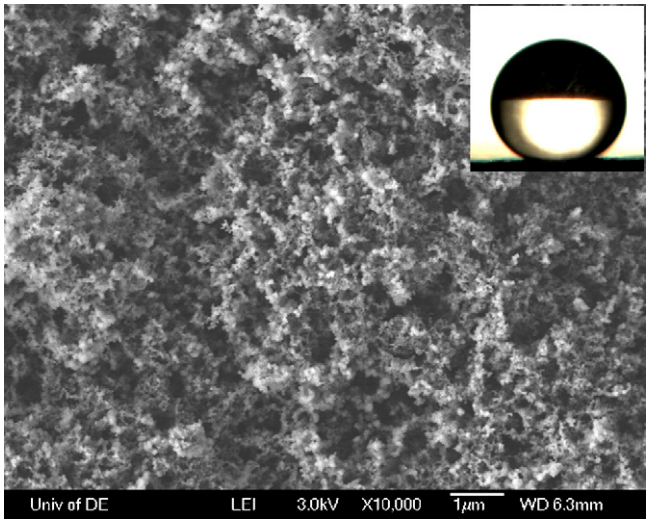

Fig. 4. SEM image of microporous layer on copper gas diffusion layer. The image at upper-right corner shows contact angle of liquid water on MPL.

pore distribution ranges from 100 nm to 1000 nm. As shown in Fig. 5 with square symbols, the cell performance improves from 0.3 W cm^{-2} to 0.45 W cm^{-2} under the same stoichiometry of 2/2. This is attributed to the reduction in internal resistance and improved water management owing to the presence of the MPL [32–34].

The developed copper GDL only has straight pores which restricts its in-plane transport. As a result, the reaction can occur only under the flow channel area, but not under the land (see Fig. 6a). The overall reactant access can be enhanced by reducing the contact area between the gas diffusion layer and the land region [35,36]. In addition, the cell performance can be improved by enhancing the in-plane transport as shown in Fig. 6b. The enhancement layer could be obtained, for example, by increasing

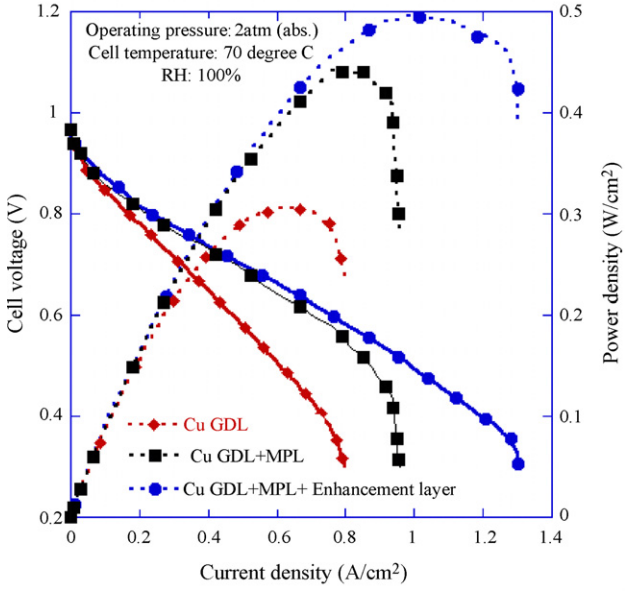

Fig. 5. Performance improvement with microporous layer (MPL) and in-plane transport enhancement by addition of carbon paper between Cu GDL and bipolar plate.

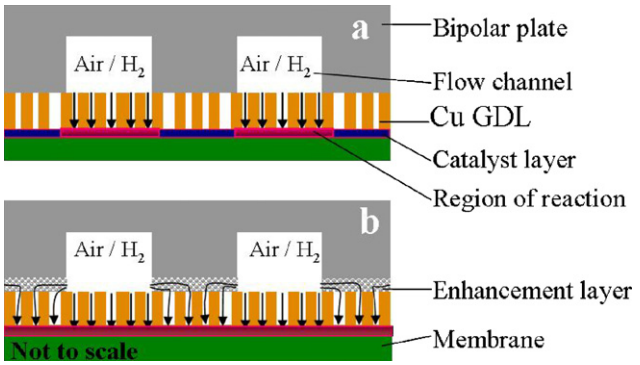

Fig. 6. Schematic for the enhancement of in-plane transport under the land. (a) Absence of enhancement layer restricts reactant access under the land; (b) addition of enhancement layer extends the region of reaction.

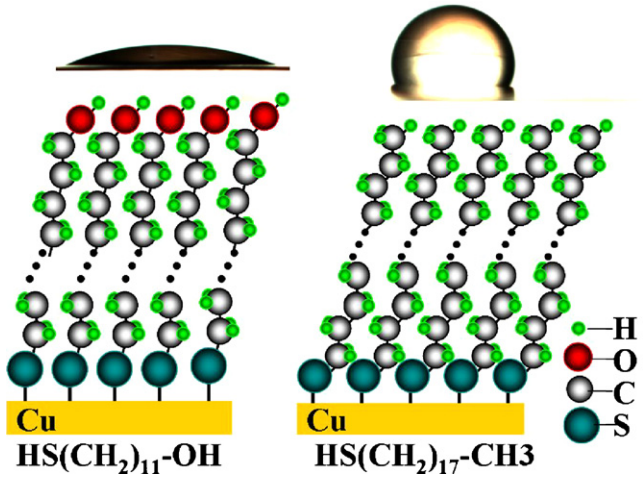

Fig. 7. Surface control of copper substrate by self-assembled monolayer.

the roughness of the contact area. The beneficial effect of the enhancement layer is shown in Fig. 5 (with circle symbols) by inserting a carbon paper GDL between the bipolar plate and the copper GDL. This additional GDL is inserted here for the purpose of demonstration only, and is not intended for use in the final design.

3.1. GDL architecture and porosity

Besides enhancing both through-plane and in-plane transports, other challenges for this nano-based material include the control of surface properties, pore shape and porosity, and the optimization of pore distribution. Two-phase transport in the pores is mainly governed by the pore geometry, surface tension of the fluid, the capillary pressure, and the wettability of the pore walls. The substrate surface of this GDL can be controlled with SAMs or by other methods [26,29]. One end of the SAM molecule binds to the copper surface via a covalent bond, while the other end points outwards. Because the exposed end of the SAM determines the surface properties, the hydrophilicity and hydrophobicity of the substrate surface can be controlled by carefully selecting the SAM head group. As shown in Fig. 7, 11-hydroxy-1-undecanethiol (HS(CH2)11OH) has a very hydrophilic OH end, while ODT (HS(CH2)17CH3) has a highly hydrophobic CH3-end. In addition, since the SAM is very thin (about 10 nm), its thermal and electrical resistances are negligible.

In hydrophobic porous media, liquid water only exists as a sphere [8,28,29,37]. Pure liquid water cannot be imbibed and will not penetrate into a pore with hydrophobic surface property (contact angle >90°) without sufficient capillary pressure, P_c, which is defined as

$$P_c = -\frac{2\sigma \cos\theta}{r}$$

where σ is the liquid surface tension, θ the contact angle of liquid water, and r is the pore radius. The liquid water fills the entire circular pore, while in non-circular cases the liquid water occupies only a partial space within the pore. Therefore, gas can be transported through the unoccupied region of the pore. This will reduce performance degradation by alleviating local flooding in the fuel cell. The pore shape can be controlled by the shape of the designed mask as shown in Fig. 8. The mask patterns of circle and ellipse are visible as dark brown regions at the center of the images, respectively. After etching, the non-

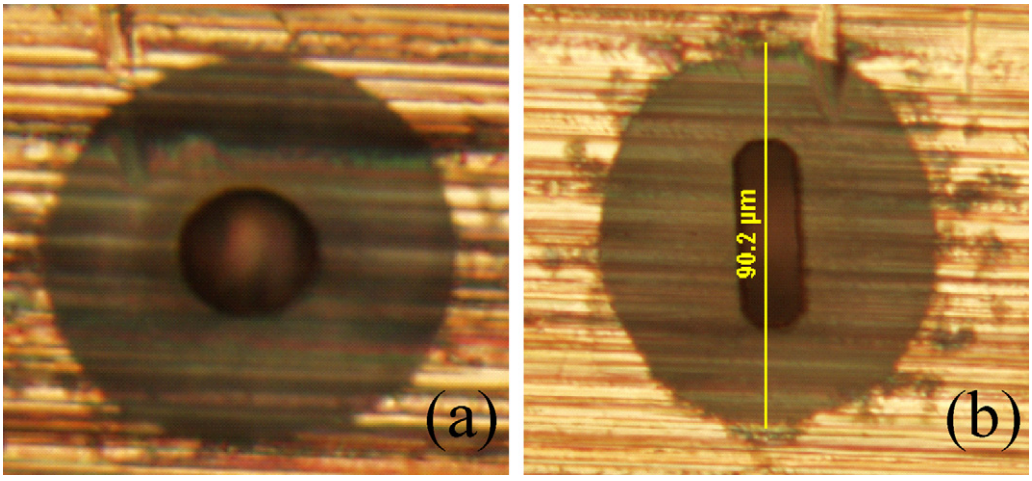

Fig. 8. The effects of mask shape on pore geometry. (a) Circular mask (center brown part) and final pore shape; (b) elliptical mask (center brown part) and final pore shape. Reproduced from Ref. [28] with permission from the Institute of Physics.

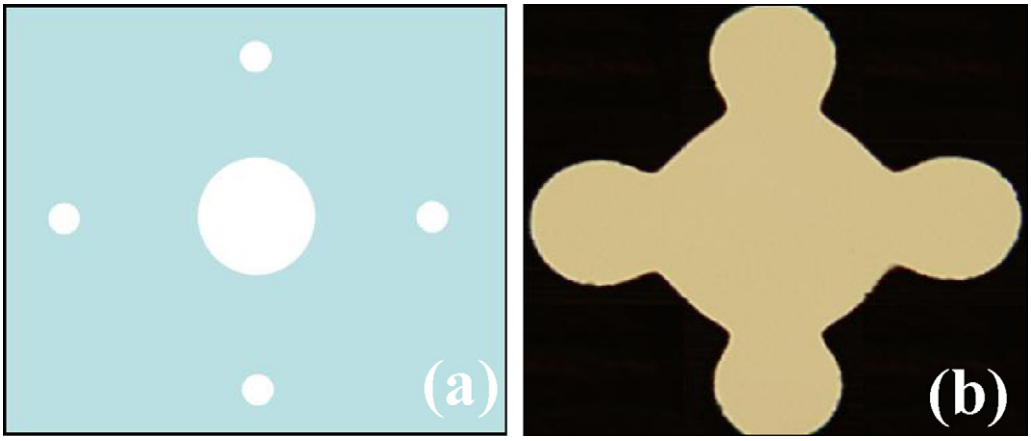

Fig. 9. Non-circular pore obtained by changing the mask pattern. (a) Mask shape; (b) final pore shape. Reproduced from Ref. [28] with permission from the Institute of Physics.

circular shape of the pore is obtained from the ellipse mask pattern in Fig. 8b.

The non-circular pore shape can be also controlled by designing the mask pattern. As shown in Fig. 9a, the five initially circular mask shapes with different sizes produce a large non-circular pore after etching as shown in Fig. 9b. It should be noted that the combination of mask shape with mask pattern would provide more efficient way to fabricate non-circular pores.

The porosity can be controlled by changing the mask size, etching time, etching rate, and pore distribution. Fig. 10 shows the porosity percentage with mask size, pore ratio and etching time. In Fig. 10a, the pore distribution of mask widths of 20 μm, 15 μm, 10 μm, 8 μm and 5 μm relative to the number density at 20 μm is 1, 1, 8, 54 and 64, respectively. After 20 min of etching, the total porosity, which is the sum of all the pores, is about 21%. With the same pore distribution, after an additional 10 min of etching, the porosity is increased from 21% to 35%. The porosity can also be obtained by varying the pore distributions as shown in Fig. 10b. The number density of mask width of 15 μm is increased from 1/128 to 54/128, while the one for 8 μm is decreased from 54/128 to 1/128. With the same etching time and the pore numbers, the total porosity is increased from 21% to 32% after 20 min of etching, and from 35% to 50% after 30 min of etching, respectively.

In this work, the concept of the metallic GDL and its feasibility in fuel cell applications are demonstrated. However, one of the future challenges is the durability of this novel GDL material. On exposure to the aggressive PEMFC environment, especially on the aerated cathode side, metallic materials are certainly subjected to corrosion and form passive films on their surface [38–43]. Dissolution of metallic ions can also occur under PEMFC operating conditions, especially under repeated cyclic through high voltages as encountered in automotive applications [44–46]. In addition, the membranes are sensitive to poisoning by metallic ions, and cell performance can degrade over long-term operation [47–49]. Significant achievements have been reported to date on the use metallic materials such as bipolar plates which face similar corrosive environments as GDLs. For example, noble metals such as gold and platinum perform similarly to graphite bipolar plates, and in some cases showed superior performance [45], while both austenitic (349TM) and ferritic (AISI446) stainless steel with high Cr content showed good corrosion resistance [38–40,47,48]. Conductive and protective coating layers are also studied in metallic bipolar plates to avoid corrosion. Both carbon-based and metal-based coatings have been investigated, and methods including physical vapor deposition, chemical vapor deposition, electroplating, and thermally growing nitride coatings have been demonstrated [49–51].

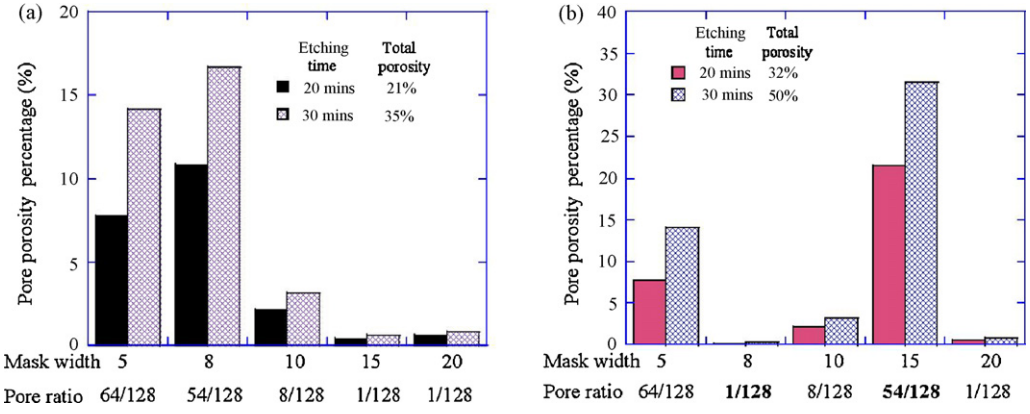

Fig. 10. Porosity controlled by changing etching time and pore distribution.

The future development of metallic GDLs can benefit from such studies of metallic bipolar plates in fuel cells.

4. Summary

A new porous gas diffusion medium with improved thermal and electrical conductivities and controllable porosity was fabricated from a metal foil using micro/nano technology, and its application in PEM fuel cells was demonstrated. As an example, the gas diffusion medium, made of 12.5 μm thick copper foil, was tested in an operational fuel cell. The performance of the novel GDL was enhanced by applying an MPL on it, and by enhancing the in-plane transport. Further improvements of the GDL, such as pore shape, porosity, and surface properties, are underway. In addition, since this novel designed material exhibits multi-functionality such as high thermal and electrical conductivities, and controllable permeability, future designs could integrate the GDL, current collector and flow field to be manufactured seamlessly by automated MEMS processes. This nano-based GDL can also be expected to facilitate *in situ* fundamental study of water management with precise control of its important parameters.

Acknowledgments

This work was supported by the Federal Transit Administration (grant FTA JPP-05-DE-03-7001) and Delaware Department of Natural Resources and Environmental Control. The help from H. Fattah and K. Malik are greatly appreciated. A portion of this work was performed in Center for Composite Materials at the University of Delaware, and at the Cornell Nanoscale Science & Technology Facility, a member of the National Nanotechnology Infrastructure Network which is supported by the National Science Foundation (grant ECS 03-35765). Figs. 2, 8 and 9 have been reproduced from [28] with permission from IOP Publishing Limited.

References

[1] N. Demirdöven, J. Deutch, Science 305 (2004) 974–976.
[2] M.F. Mathias, J. Roth, J. Fleming, W. Lehnert, in: W. Vielstich, A. Lamm, H.A. Gasteiger (Eds.), Handbook of Fuel Cells—Fundamentals, Technology and Applications, vol. 3, John Wiley & Sons, 2003, pp. 517–537.
[3] F.Y. Zhang, D. Spernjak, A.K. Prasad, S.G. Advani, J. Electrochem. Soc. 154 (2007) B1152.
[4] J.J. Kowal, A. Turhan, K. Heller, J. Brenizer, M.M. Mench, J. Electrochem. Soc. 153 (2006) A1971.
[5] Z. Weber, R.M. Darling, J. Power Sources 168 (1) (2007) 191–199.
[6] T.A. Trabold, J.P. Owejan, D.L. Jacobson, M. Arif, P.R. Huffman, Int. J. Heat Mass Transfer 49 (2006) 4712.
[7] Y. Wang, C.Y. Wang, K.S. Chen, Electrochim. Acta 52 (12) (2007) 3965–3975.
[8] F.Y. Zhang, X.G. Yang, C.Y. Wang, J. Electrochem. Soc. 153 (2006) A225–A232.
[9] K. Jiao, B. Zhou, J. Power Sources 169 (2) (2007) 296–314.
[10] D. Spernjak, A.K. Prasad, S.G. Advani, J. Power Sources 170 (2007) 334–344.
[11] U. Pasaogullari, C.Y. Wang, J. Electrochem. Soc. 151 (2004) A399.
[12] X.G. Yang, F.Y. Zhang, A. Lubawy, C.Y. Wang, Electrochem. Solid-State Lett. 7 (2004) A408.
[13] K. Tuber, D. Pocza, C. Hebling, J. Power Sources 124 (2003) 403.
[14] Z. Weber, J. Newman, Chem. Rev. 104 (10) (2004) 4679–4726.
[15] S. Litster, C.R. Buie, T. Fabian, J.K. Eaton, J.G. Santiago, J. Electrochem. Soc. 154 (10) (2007) B1049–B1058.
[16] N. Pekula, K. Heller, P.A. Chuang, A. Turhan, M.M. Mench, J.S. Brenizer, K. Unlu, Nucl. Instrum. Methods Phys. Res. A 542 (2005) 134.
[17] K. Nishida, T. Murakami, S. Tsushima, Electrochemistry 75 (2) (2007) 149–151.
[18] T. Murahashi, H. Kobayashi, E. Nishiyama, Electrochemistry 75 (2) (2007) 261–263.
[19] E. Passalacqua, G. Squadrito, F. Lufrano, A. Patti, L. Giorgi, J. Appl. Electrochem. 31 (2001) 449.
[20] J. Benziger, J. Nehlsen, D. Blackwell, T. Brennan, J. Itescu, J. Membr. Sci. 261 (1/2) (2005) 98–106.
[21] W.K. Lee, C.H. Ho, J.W. Van Zee, M. Murthy, J. Power Sources 84 (1999) 45.
[22] G. Lin, T.V. Nguyen, J. Electrochem. Soc. 152 (2005) A1942.
[23] H. Meng, J. Power Sources 162 (1) (2006) 426–435.
[24] C.M. Ho, Y.C. Tai, Annu. Rev. Fluid Mech. 30 (1998) 579–612.
[25] K.R. Williams, R.S. Muller, J. Microelectromech. Syst. 5 (1996) 256–269.
[26] J.J. Gau, E.H. Lan, B. Dunn, C.M. Ho, J. Biosens. Bioelectr. 9 (12) (2001) 745–755.
[27] K. Kondo, H. Kurihara, H. Murakamia, Electrochem. Solid-State Lett. 9 (2006) C36–C37.
[28] F.Y. Zhang, A.K. Prasad, S.G. Advani, J. Micromech. Microeng. 16 (2006) 23.
[29] E.H. Lan, T.A. Umali, D. Dunn, C.M. Ho, J. Micromech. Microeng. 14 (2003) 91–95.
[30] Q.L. Dong, J. Kull, M.M. Mench, J. Power Sources 139 (2005) 106.
[31] Z. Qi, A. Kaufman, J. Power Sources 109 (2002) 38.
[32] F.Q. Liu, G.Q. Lu, C.Y. Wang, J. Electrochem. Soc. 153 (2006) A543.
[33] S. Park, J.-W. Lee, B.N. Popov, J. Power Sources 163 (2006) 1.
[34] Z. Weber, J. Newman, J. Electrochem. Soc. 152 (4) (2005) A677–A688.
[35] T.A. Trabold, Heat Transfer Eng. 26 (2005) 3.
[36] D.P. Wilkinson, M. Blanco, H. Zhao, J. Wu, H. Wang, Electrochem. Solid-State Lett. 10 (2007) 9.
[37] E.C. Kumbur, K.V. Sharp, M.M. Mench, J. Power Sources 168 (2006) 2.
[38] P. Brady, B. Yang, H. Wang, J.A. Turner, K.L. More, M. Wilson, F. Garzon, JOM 58 (2006) 50–57.
[39] H. Wang, G. Teeter, J.A. Turner, J. Electrochem. Soc. 152 (3) (2005) B99–B104.
[40] R.J. Tian, J.C. Sun, L. Wang, J. Power Sources 163 (2007) 719–724.
[41] E.A. Cho, U.-S. Jeon, S.-A. Hong, I.-H. Oh, S.-G. Kang, J. Power Sources 142 (2005) 177.
[42] H. Tawfik, Y. Hung, D. Mahajan, J. Power Sources 163 (2) (2007) 755–767.
[43] A. Hermann, T. Chaudhuri, P. Spagnol, Int. J. Hydrogen Energy 30 (2005) 1297.
[44] C.L. Ma, S. Warthesen, D.A. Shores, J. New Mater. Electrochem. Syst. 3 (2000) 221.
[45] J. Wind, R. Spah, W. Kaiser, G. Bohm, J. Power Sources 105 (2002) 256.
[46] N.P. Brandon, S. Skinner, B.C.H. Steele, Ann. Rev. Mater. Res. 33 (2003) 183.
[47] D.P. Davies, P.L. Adcock, M. Turpin, S.J. Rowen, J. Power Sources 86 (2000) 237.
[48] V. Mehta, J.S. Cooper, J. Power Sources 144 (2003) 32–53.
[49] H. Wang, M.A. Sweikart, J.A. Turner, J. Power Sources 115 (2003) 243–251.
[50] H. Wang, J.A. Turner, J. Power Sources 128 (2004) 193–200.
[51] S. Lee, C. Huang, J. Lai, Y. Chen, J. Power Sources 131 (2004) 162.